Electronic Supplementary Material (ESI) for Journal of Materials Chemistry A.

Electronic Supplementary Information

Table of Contents

Table S1 contains oxygen storage capacities (in wt%) observed for samples at all tested temperatures. Values highlighted in yellow are the highest values at their given temperature. Blank spaces represent unperformed experiments on the x = 0.35 and 0.40 samples given their much lower oxygen capacities overall.

		Temperature (°C)					
		400	**450**	**500**	**550**	**600**	**700**
Ca^{2+} ratio (x)	**0.00**	0.84	0.82	0.95	1.06	1.30	1.40
	0.05	0.81	0.91	1.19	1.37	1.69	1.55
	0.10	0.93	1.08	1.91	2.04	1.90	1.50
	0.15	1.35	2.17	2.26	2.04	1.83	1.44
	0.20	2.10	2.37	2.19	1.99	1.78	1.36
	0.25	2.41	2.35	2.13	1.84	1.43	0.49
	0.30	2.41	2.21	1.77	0.54	0.24	0.14
	0.35	2.13	1.90	0.46			
	0.40	1.72					

Table S2 contains the time, in minutes, required to release **90%** of the overall oxygen release for each experiment shown in the main text in Figure 4. The time decreases as a sample is cycled at higher temperature, or a sample with a higher Ca content is compared isothermally to another. Exceptions occur when the amount of oxygen cycled is much lower.

		Temperature (°C)					
		400	**450**	**500**	**550**	**600**	**700**
Ca^{2+} ratio	**0.00**	9.56	16.53	17.38	13.93	15.58	15.15
	0.05	31.77	18.33	20.70	16.03	15.65	11.67
	0.10	36.03	22.08	25.08	15.47	8.85	4.93
	0.15	51.35	24.22	11.83	5.35	3.02	1.68
	0.20	45.17	17.85	6.53	3.00	1.70	0.90
	0.25	36.13	7.00	2.18	1.00	0.53	1.05
	0.30	25.83	4.10	1.17	0.70	4.72	17.32
	0.35	16.03	3.00	1.07			
	0.40	10.30					

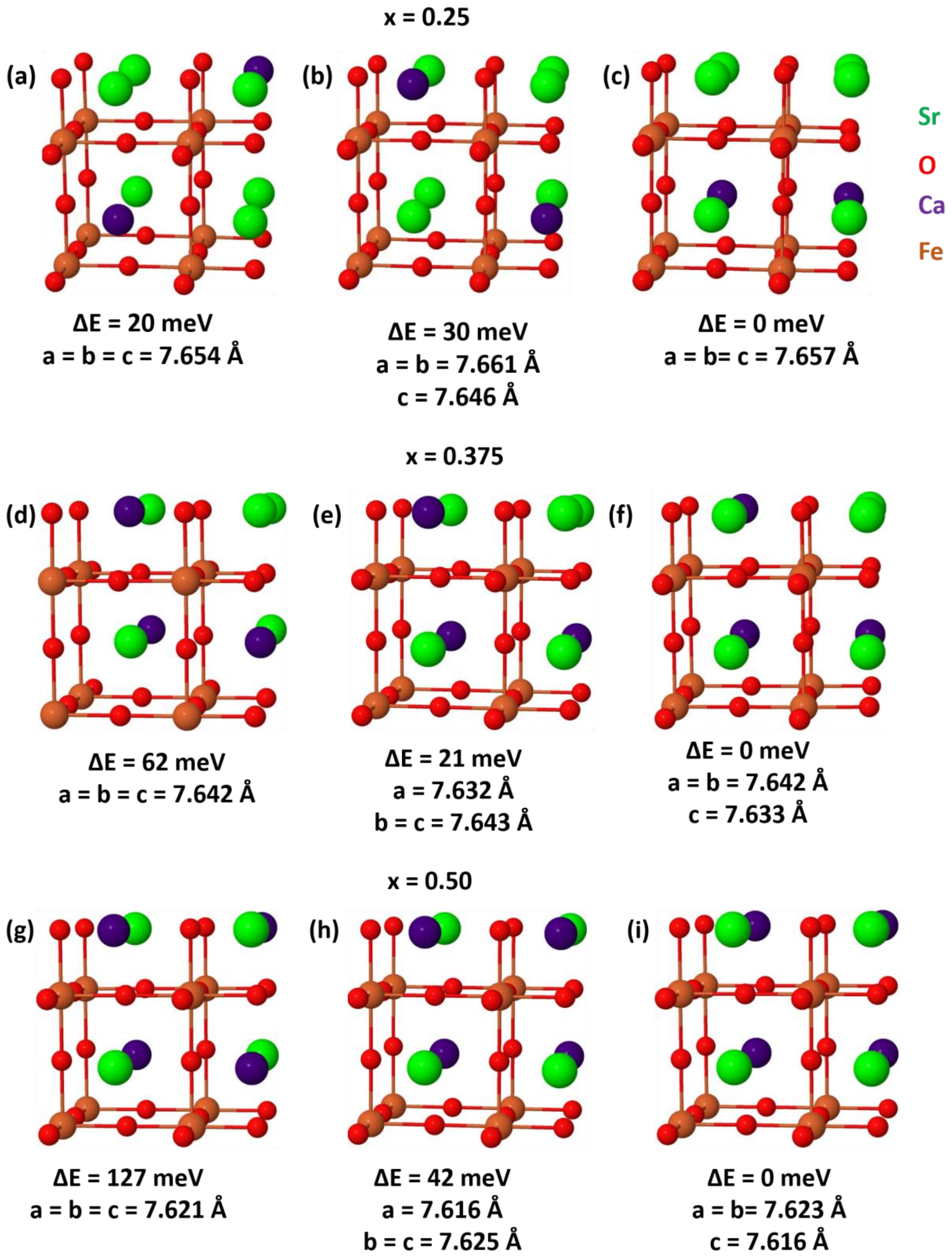

Figure S1. Optimized structures of $Sr_{1-x}Ca_xFeO_3$. The energies are given with respect to the lowest energy structure at each Ca concentration. The lowest energy structures have a ΔE = 0.

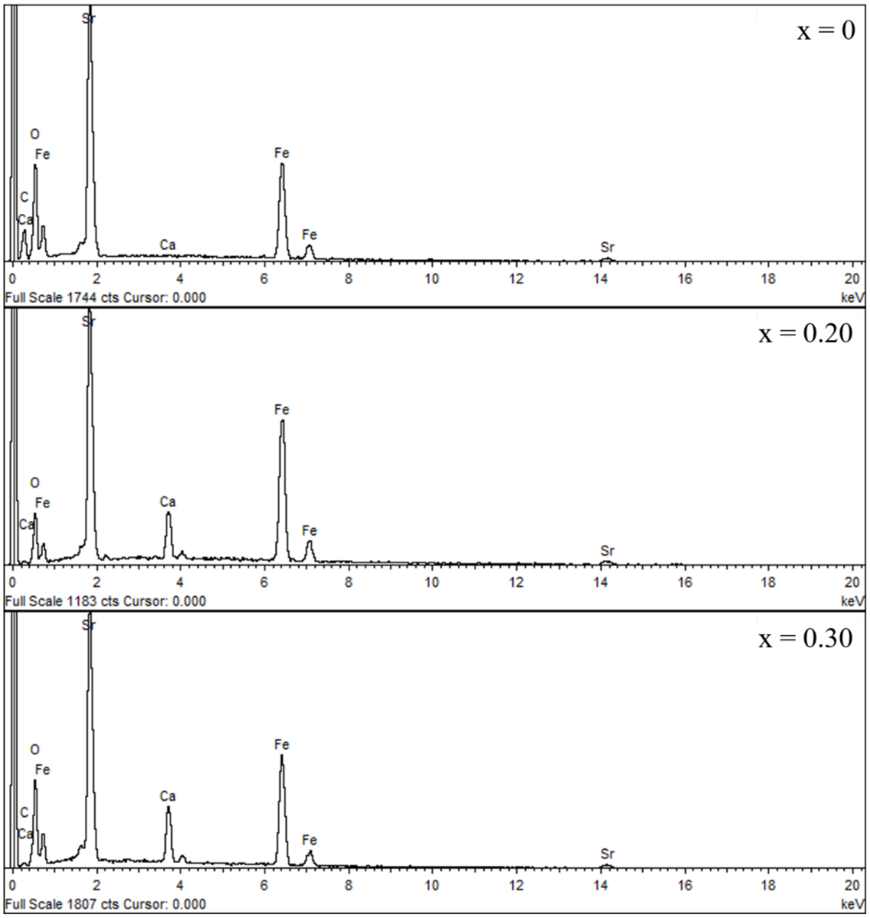

$Sr_{1-x}Ca_xFeO_3$	x [Ca/(Ca+Sr)]	A-site/B-site
x = 0.00	0.00205 ± 0.0027	0.831 ± 0.28
x = 0.05	0.050 ± 0.004	1.13 ± 0.14
x = 0.10	0.098 ± 0.010	1.02 ± 0.16
x = 0.15	0.144 ± 0.023	1.09 ± 0.16
x = 0.20	0.206 ± 0.018	0.88 ± 0.14
x = 0.25	0.247 ± 0.028	1.00 ± 0.18
x = 0.30	0.273 ± 0.013	1.08 ± 0.05
x = 0.35	0.409 ± 0.068	1.01 ± 0.25
x = 0.40	0.581 ± 0.164	0.63 ± 0.39

Figure S2 contains the SEM-EDS spectra collected for a selection of our $Sr_{1-x}Ca_xFeO_3$ systems, specifically x = 0, 0.20, and 0.30. The table underneath lists the atomic ratios calculated from the EDS experiments performed. Five distinct locations were selected for each sample to control irregularities in the EDS spectra. The Ca:(Ca+Sr) and A:B ratios largely agree with the ratios of starting metal precursors. Disagreements are mostly limited to systems that are clearly multiphase by XRD (x > 0.30).

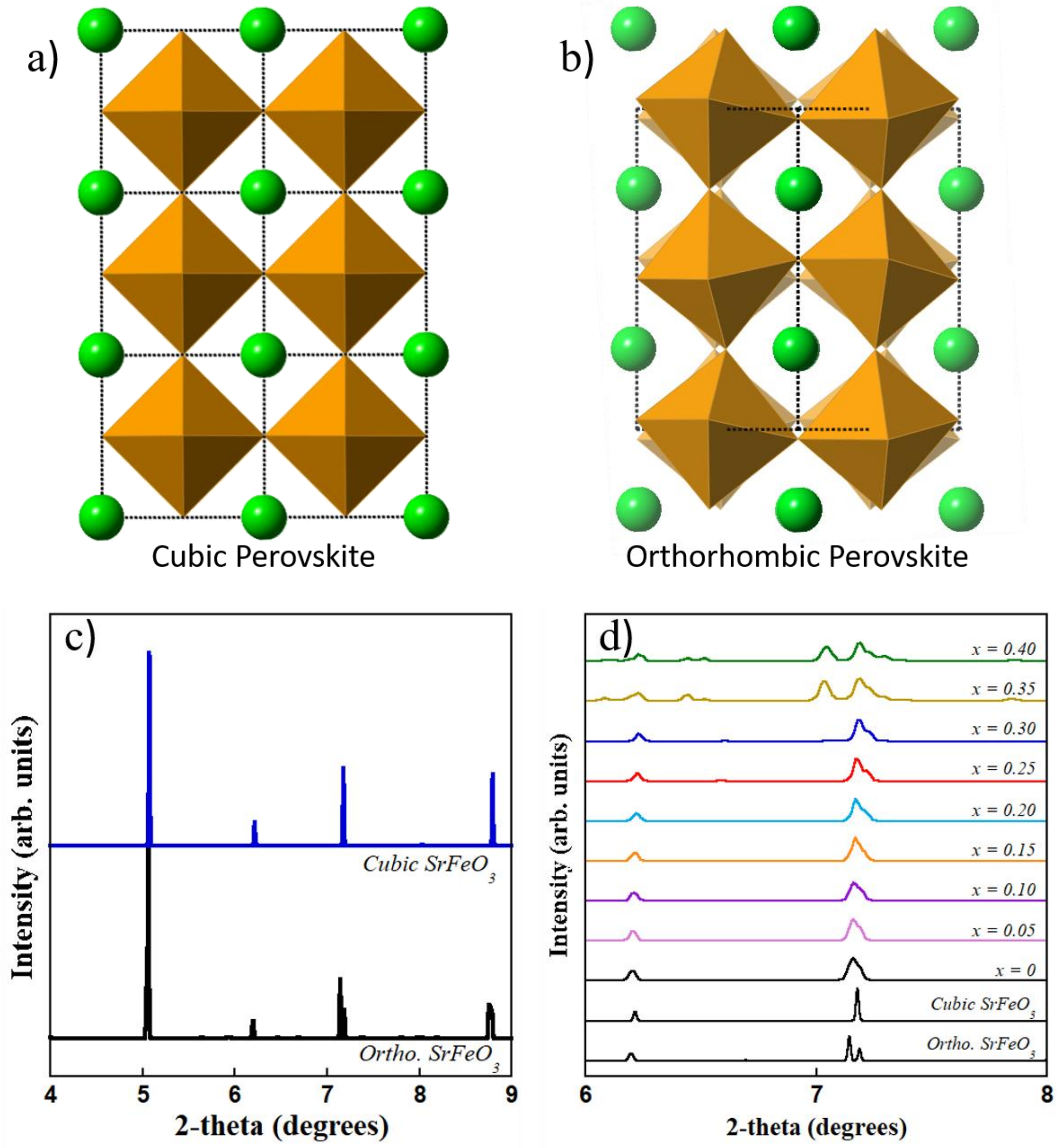

Figure S3 displays the crystal structure of a) cubic $SrFeO_3$ and b) orthorhombic $SrFeO_3$. This structures only differ by a slight tilt in the component FeO_6 octahedra. This similarity is also found in c) their powder X-ray diffraction patterns. While the simulated cubic structure leads to a simple pattern with gaussian broadening, the orthorhombic structure yields a slightly more complex pattern due to symmetry-breaking FeO_6 rotation. When observing both patterns versus our samples, specifically around 7 degrees 2-theta, our samples exhibit patterns in greater agreement with the orthorhombic phase. This minor distinction allows for slightly better Rietveld refinement fittings, due to the additional parameters that are able to be fitting in the less-symmetric structure.

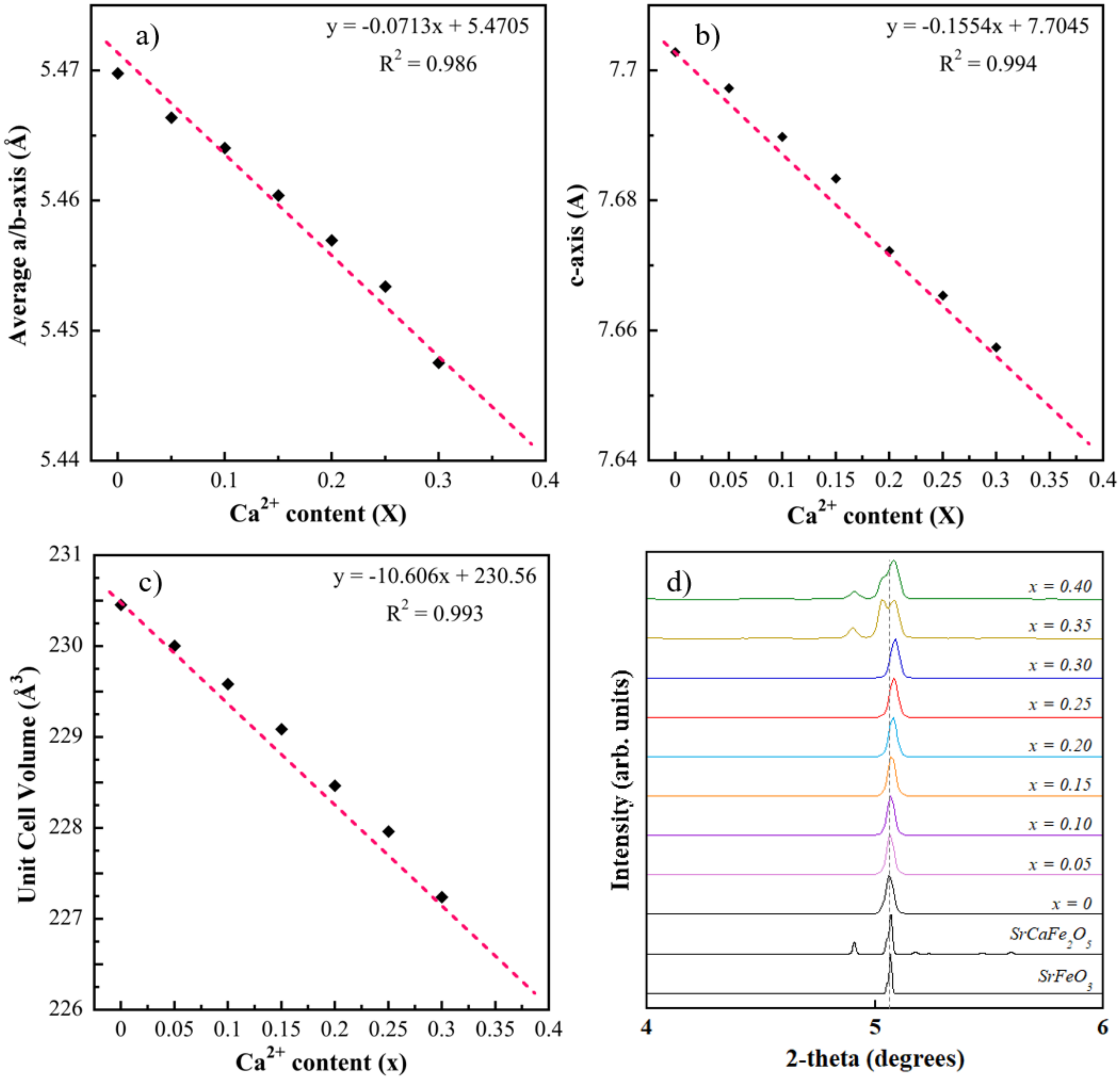

Figure S4 displays the relationship between a) the average a and b length, b) the c length, and c) unit cell volume all refined through Rietveld analysis of the powder X-ray diffraction data, versus the Ca content in the $Sr_{1-x}Ca_xFeO_{3-\delta}$ samples synthesized. The observed shift in the major reflection for the perovskite phase is displayed in d). Small deviations away from linear regression could be due to a variety of factors, including different non-stoichiometry (δ) values, heterogeneity of Ca content, and the presence of a secondary phase.

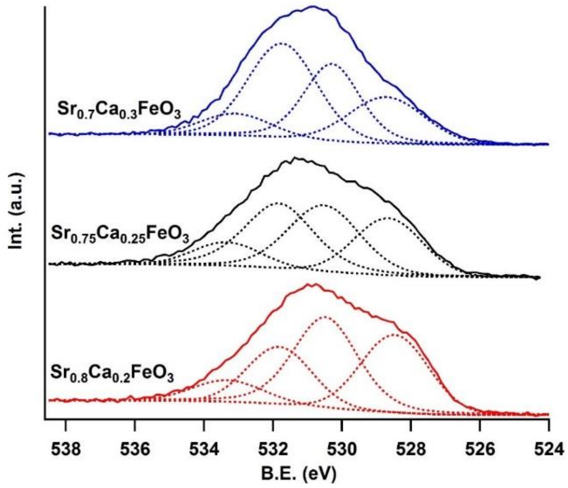

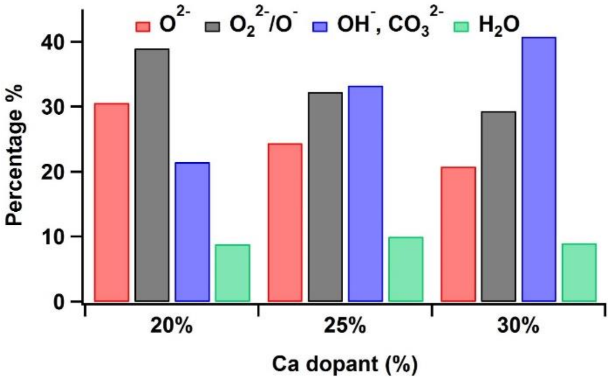

Sample	**Lattice O^{2-}**		**Surf. O$_2^{2-}$/O$^-$**		**Ads. OH$^-$, CO$_3^{2-}$**		**Ads. H$_2$O**	
	BE (eV)	**Ratio**	**BE (eV)**	**Ratio**	**BE (eV)**	**Ratio**	**BE (eV)**	**Ratio**
Sr$_{0.8}$Ca$_{0.2}$FeO$_3$	528.5	30.6%	530.5	39.0%	531.8	21.5%	533.3	8.9%
Sr$_{0.75}$Ca$_{0.25}$FeO$_3$	528.7	24.4%	530.5	32.2%	531.8	33.3%	533.3	10.0%
Sr$_{0.7}$Ca$_{0.3}$FeO$_3$	528.7	20.8%	530.3	29.4%	531.7	40.8%	533.1	9.0%

Figure S5 contains the XPS spectra corresponding to the O 1s. We were able to fit the spectra of each Sr$_{1-x}$Ca$_x$FeO$_{3-\delta}$ sample using the oxygen species determinations found in Merino, et. al., App. Surf. Sci. **2006**, 253, 1489-1493. The amount of lattice O^{2-} and surface O$_2^{2-}$/O$^-$ decreases as the Ca^{2+} content is increased, whereas the amount of adsorbed OH$^-$/CO$_3^{2-}$ is increased. This suggests that the lattice and surface oxygen is more labile in the higher Ca^{2+} content samples, which agrees with our experimental findings.

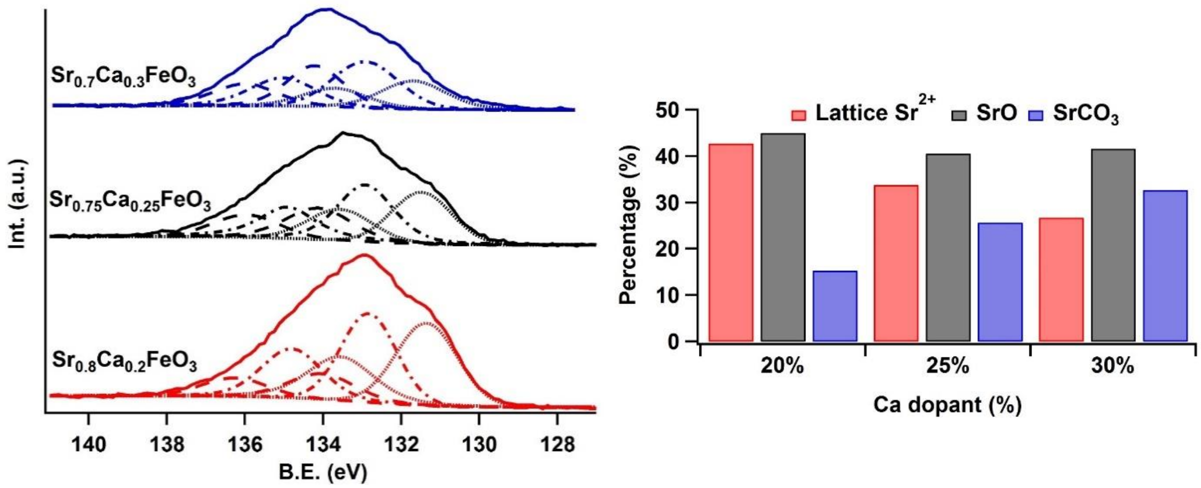

Sample	Lattice Sr^{2+}			SrO			$SrCO_3$		
	$3d^{5/2}$ BE (eV)	$3d^{3/2}$ BE (eV)	Ratio	$3d^{5/2}$ BE (eV)	$3d^{3/2}$ BE (eV)	Ratio	$3d^{5/2}$ BE (eV)	$3d^{3/2}$ BE (eV)	Ratio
$Sr_{0.8}Ca_{0.2}FeO_3$	131.4	133.6	42.7%	132.8	134.8	45.0%	134.0	136.3	15.3%
$Sr_{0.75}Ca_{0.25}FeO_3$	131.5	133.6	33.8%	132.9	134.9	40.6%	134.1	136.0	25.7%
$Sr_{0.7}Ca_{0.3}FeO_3$	131.7	133.7	26.7%	132.9	135.0	41.6%	134.2	136.0	32.7%

Figure S6 contains the Sr 3d XPS spectra for the three $Sr_{1-x}Ca_xFeO_{3-\delta}$ samples. Like the O 1s for these samples, an increase in the Ca^{2+} content leads to increased adsorbed CO_3^{2-} and decreased lattice Sr^{2+}.

Sample	Desorp. Max (°C)	Volume O_2 (mL/g)
x = 0.00	…	17.134
x = 0.05	626.6	16.282
x = 0.10	574.8	16.264
x = 0.15	531.6	15.292
x = 0.20	502.3	15.678
x = 0.25	468.5	13.718
x = 0.30	416.1	14.388
x = 0.35	399.2	13.262
x = 0.40	388.5	11.482

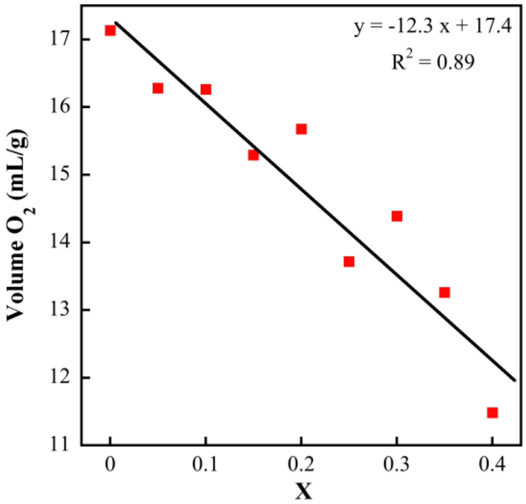

Figure S7 lists the temperature of maximum O_2 desorption and the total O_2 release between 200-1000°C for the $Sr_{1-x}Ca_xFeO_3$ series (x = 0-0.40), as measured during O_2-TPD and the plot visualizes the total O_2 release. Overall, the addition of Ca to the lattice causes a decrease in the volume of oxygen released.

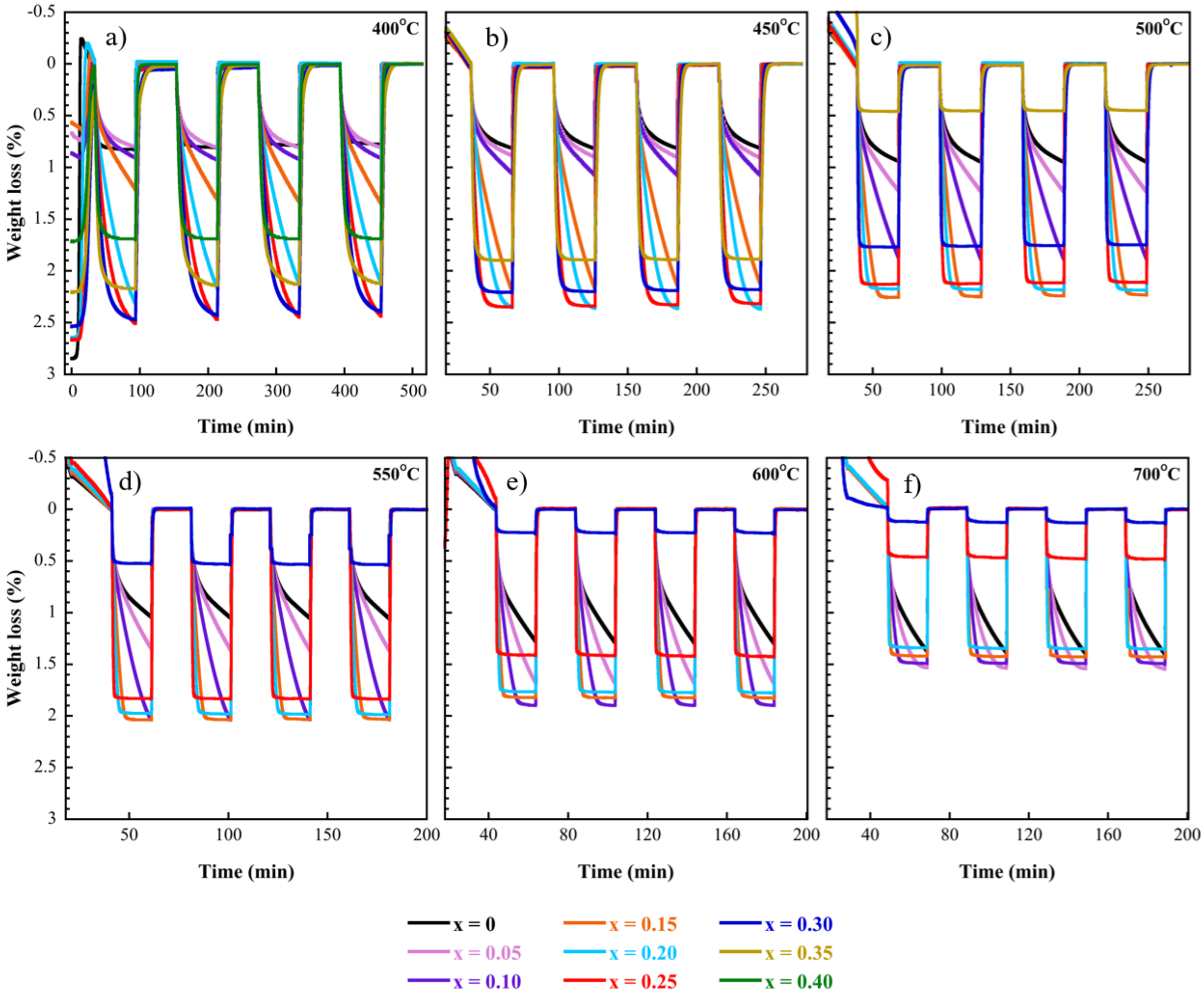

Figure S8 displays extended isothermal TGA cycling studies for a selection of $Sr_{1-x}Ca_xFeO_{3-\delta}$ systems. A total of 4 cycles is shown for each experiment with little to no degradation in performance observed. This promising stability is inherent to the minimal structural rearrangement necessary for perovskite oxygen carrying materials during O_2 uptake and release.

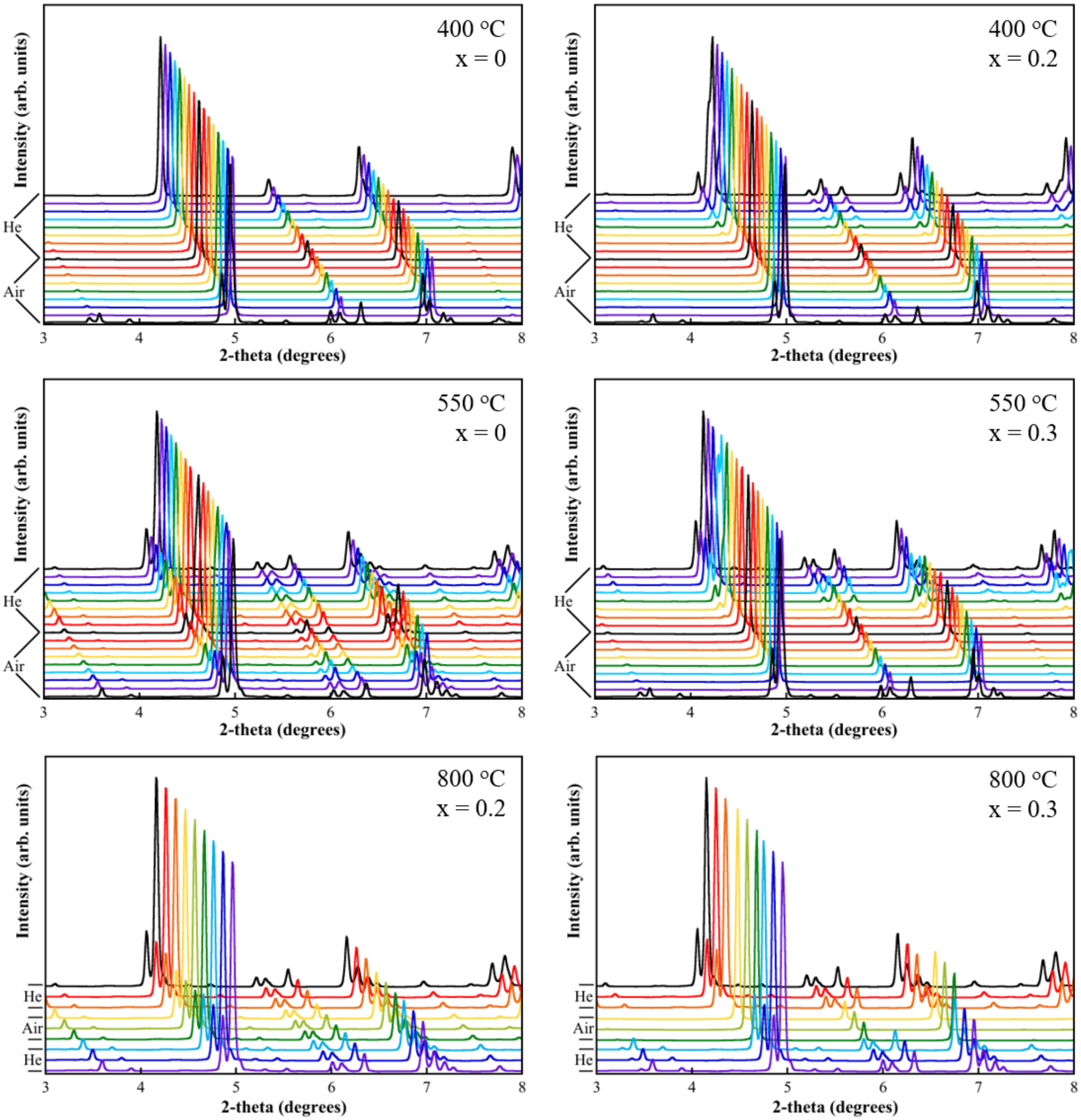

Figure S9 displays a condensed collection of synchrotron powder X-ray diffraction patterns from *in situ* high-temperature air/He cycling experiments. The top row contains data collected on $SrFeO_3$ (left) and $Sr_{0.8}Ca_{0.2}FeO_3$ (right) from experiments performed at 400 °C. The first pattern was obtained under He flow, followed by eight patterns under air flow and then He flow, collected 3 minutes apart.

The middle row contains data collected on $SrFeO_3$ (left) and $Sr_{0.7}Ca_{0.3}FeO_3$ (right) from experiments performed at 550 °C. The first pattern was obtained under He flow, followed by eight patterns under air flow and then He flow, collected 2 minutes apart.

The bottom row contains data collected on $Sr_{0.8}Ca_{0.2}FeO_3$ (left) and $Sr_{0.7}Ca_{0.3}FeO_3$ (right) from experiments performed at 800 °C. The first three patterns were collected under He, followed by 3 each under air and He. Total dwell time at each gas – 10 minutes.

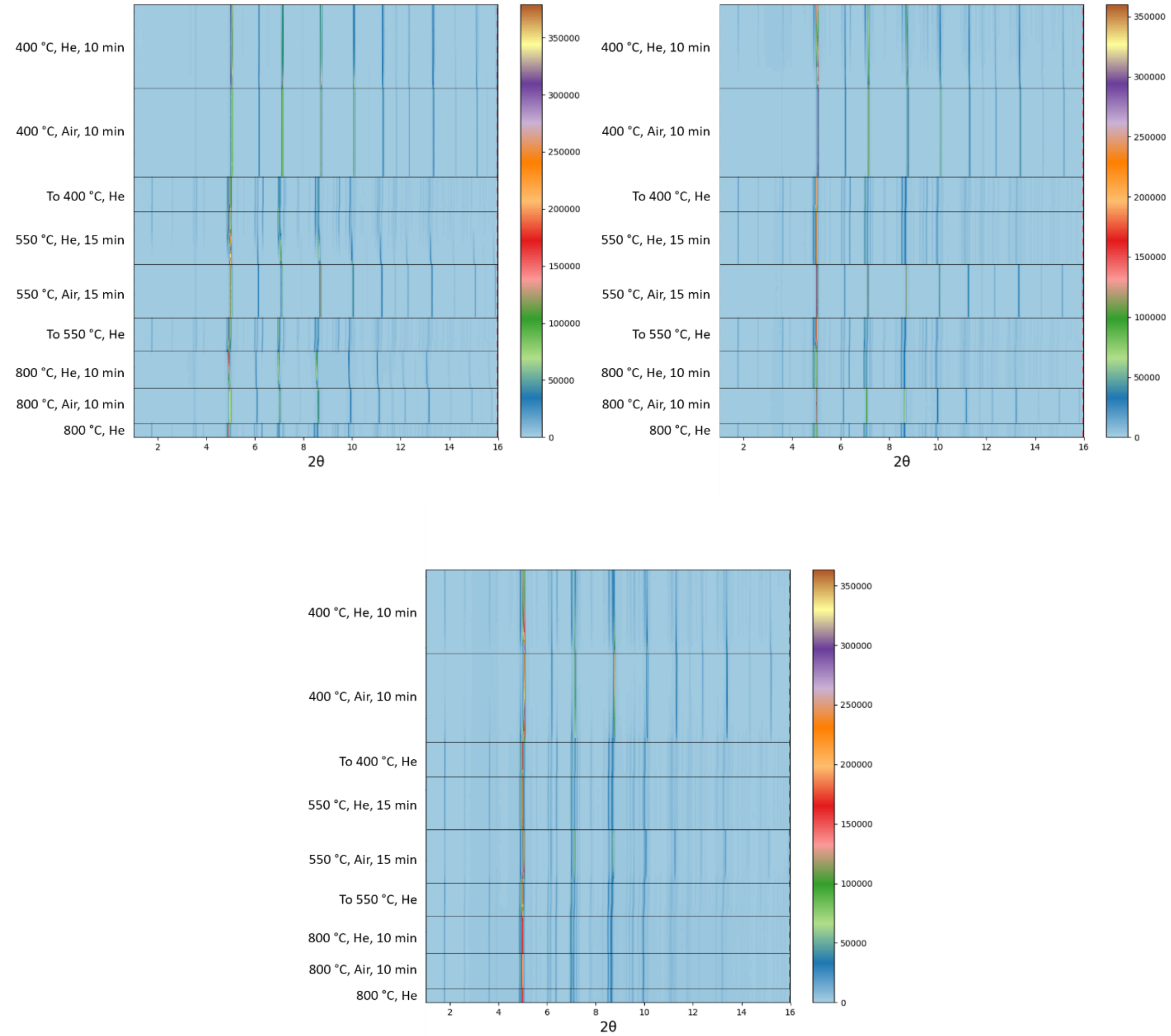

Figure S10 contains contour plots showing the sequence of gas switching experiments performed at the Advanced Photon Source. Data includes approximately 120 patterns each performed 1 minute apart. Horizontal lines are used to represent changes in temperature ramp or gas flow. Top left – $SrFeO_3$, Top Right – $Sr_{0.8}Ca_{0.2}FeO_3$, Bottom – $Sr_{0.7}Ca_{0.3}FeO_3$.